

## 2,2,2-Trifluoroethanol Changes the Transition Kinetics and Subunit Interactions in the Small Bacterial Mechanosensitive Channel MscS

Bradley Akitake,\* Robin E. J. Spelbrink,<sup>†</sup> Andriy Anishkin,\* J. Antoinette Killian,<sup>†</sup> Ben de Kruijff,<sup>†</sup> and Sergei Sukharev\*

\*Department of Biology, University of Maryland, College Park, Maryland; and <sup>†</sup>Department of Biochemistry of Membranes, Institute of Biomembranes, Utrecht University, Utrecht, The Netherlands

**ABSTRACT** 2,2,2-Trifluoroethanol (TFE), a low-dielectric solvent, has recently been used as a promising tool to probe the strength of intersubunit interactions in membrane proteins. An analysis of inner membrane proteins of *Escherichia coli* has identified several SDS-resistant protein complexes that separate into subunits upon exposure to TFE. One of these was the homo-heptameric stretch-activated mechanosensitive channel of small conductance (MscS), a ubiquitous component of the bacterial turgor-regulation system. Here we show that a substantial fraction of MscS retains its oligomeric state in cold lithium-dodecyl-sulfate gel electrophoresis. Exposure of MscS complexes to 10–15 vol % TFE in native membranes or nonionic detergent micelles before lithium-dodecyl-sulfate electrophoresis results in a complete dissociation into monomers, suggesting that at these concentrations TFE by itself disrupts or critically compromises intersubunit interactions. Patch-clamp analysis of giant *E. coli* spheroplasts expressing MscS shows that exposure to TFE in lower concentrations (0.5–5.0 vol %) causes leftward shifts of the dose-response curves when applied extracellularly, and rightward shifts when added from the cytoplasmic side. In the latter case, TFE increases the rate of tension-dependent inactivation and lengthens the process of recovery to the resting state. MscS responses to pressure ramps of different speeds indicate that in the presence of TFE most channels reside in the resting state and only at tensions near the activation threshold does TFE dramatically speed up inactivation. The effect of TFE is reversible as normal channel activity returns 15–30 min after a TFE washout. We interpret the observed midpoint shifts in terms of asymmetric partitioning of TFE into the membrane and distortion of the bilayer lateral pressure profile. We also relate the increased rate of inactivation and subunit separation with the capacity of TFE to perturb buried interhelical contacts in proteins and discuss these effects in the framework of the proposed gating mechanism of MscS.

### INTRODUCTION

Since the mid-1960s, halogenated alcohols such as 2,2,2-trifluoroethanol (TFE) have been known to exert strong effects on protein secondary structure. More recently, these solvents have found new applications in the study of membrane proteins. Having a lower dielectric constant than water (1), TFE is often chosen as a nonpolar medium for spectroscopic determination of peptide conformations (2–4) and helical propensities (5,6). TFE also serves as a nonpolar cosolvent in studies of conformational equilibria and protein folding kinetics (7,8).

Although TFE is fully miscible with water at any ratio, the molecule forms microscopic clusters in aqueous solutions with the highest propensity for aggregation near 30 vol % (1,9). At these concentrations, TFE strongly stabilizes the  $\alpha$ -helical and  $\beta$ -sheet structures of many soluble and amphiphilic peptides by reducing solvation of the backbone amide groups thus destabilizing extended coil conformations (10,11). TFE has also been proposed to associate with apolar side chains, providing a nonaqueous matrix for the hydrophobic collapse of polypeptides (12–14). TFE was shown to stabilize the secondary and tertiary structures of globular

proteins subjected to denaturing agents or elevated temperatures (15). Finally, TFE has been shown to accelerate protein folding (7) and disfavor partially folded intermediates even at low concentrations (8).

In contrast to the stabilizing effects observed in soluble proteins, TFE predominantly destabilizes integral membrane proteins and their complexes. The bacterial potassium channel KcsA has been well studied in this regard. KcsA retains its tetrameric structure in nonionic detergents and even in SDS (16); however, it is completely disrupted into monomers by 20 vol % TFE present in a DDM detergent solution (17). Further increase of TFE to 35 vol % under such conditions leads to a reversible loss of secondary structure (18). Surrounding phospholipids, especially PE, stabilize the liposome-reconstituted KcsA complex against TFE, despite the fact that TFE concentrations above 20 vol % severely perturb membranes themselves (17).

TFE's ability to separate hydrophobic polypeptide chains has been utilized to improve the quality of samples for two-dimensional electrophoresis of membrane protein mixtures (19,20). More recently, a new proteomic approach to identify partners in stably associated detergent-resistant complexes has been designed. In this procedure, a change of protein mobility in gels upon exposure to TFE indicated that the components had altered their oligomeric state (21). Such analysis of the *Escherichia coli* inner membrane has

Submitted October 3, 2006, and accepted for publication January 9, 2007.

B. Akitake and R. E. J. Spelbrink contributed equally to this work.

Address reprint requests to Sergei Sukharev, Tel.: 301-405-6923; E-mail: sukharev@umd.edu.

© 2007 by the Biophysical Society

0006-3495/07/04/2771/14 \$2.00

doi: 10.1529/biophysj.106.098715

identified ~60 oligomeric proteins. One of these proteins is the mechanosensitive channel of small conductance (MscS), a ubiquitous component of the bacterial osmoregulation system and a highly convenient model system for mechanistic studies of mechanosensitive channel gating.

MscS, a product of *E. coli mscS* (formerly *yggB*) gene, is a stretch-activated (mechanosensitive) channel that acts as a release valve for small intracellular osmolytes in the event of acute osmotic downshock (22). Purification and reconstitution experiments proved that the channel opens in response to membrane tension transmitted directly through the lipid bilayer (23,24). Functional patch-clamp analysis of MscS responses to pulses of hydrostatic pressure across the membrane indicate an adaptive multistate behavior, featuring tension-dependent transitions from the resting to open and then to inactivated states (22,25,26). The solved three-dimensional structure of MscS (27) revealed a heptameric assembly of identical subunits, each comprised of three transmembrane helices (TM1–TM3). The C-terminal ends of each subunit contribute to a large, hollow, cytoplasmic domain. The third transmembrane helix (TM3) lines the conducting pore and bears a characteristic kink at the cytoplasmic side (27). The MscS crystal structure laid the groundwork for several hypotheses about its gating mechanism, with proposed conformational transitions of either smaller (28) or larger scale (26,29,30). Thermodynamic analysis of dose-response curves, however, strongly suggested that the lateral protein expansion associated with the opening transition is large (~8–18 nm<sup>2</sup>) and must involve a substantial rearrangement of interhelical interactions (23,26).

In this work, we studied the oligomerization state and functional behavior of MscS in the presence of TFE. We report the conditions at which oligomeric MscS complexes remain stable in the presence of ionic detergents and the range of TFE concentrations at which breakdown into individual subunits occurs. We provide the first evidence that TFE, at concentrations much lower than those required for subunit separation, changes the equilibrium and transition kinetics between the functional states by reversibly driving the channel into the inactivated state. This new data suggests that TFE can be used for controlled perturbations of interhelical interactions in functional studies of membrane proteins.

## METHODS

### Materials

Electrophoresis setups were purchased from Bio-Rad Laboratories (Emmen, The Netherlands). Lithium dodecyl sulfate (LDS) was purchased from USB (Cleveland, OH). Octylglucoside was obtained from LabScientific (Livingston, NJ). Ni<sup>2+</sup> nitrilotriacetic acid agarose was obtained from Qiagen Benelux N.V. (The Netherlands). Anti-his<sub>6</sub>-C-term antibodies were purchased from Invitrogen (The Netherlands). Isopropyl- $\beta$ -D-thiogalactopyranoside was obtained from Calbiochem (Los Angeles, CA). 2,2,2-Trifluoroethanol (TFE) was purchased from Merck (Darmstadt, Germany). 1,1,1,3,3,3-hexafluoroisopropanol was purchased from Acros Organics (Deventer, The Netherlands). Coomassie Brilliant Blue G-250 was purchased from ICN

Biomedicals (Aurora, OH). Lithium dodecyl sulfate-polyacrylamide gel electrophoresis (LDS-PAGE) gradient gels were cast using a Hoefner SG30 gel maker while nongradient LDS gels were cast on BioRad Protean III casting systems. All other chemicals were of the highest quality commercially available.

### Strains and expression constructs

PB111, a plasmid containing MscS with a C-terminal <sub>6</sub>His tag, was a gift of Dr. Paul Blount (UT Southwestern, Dallas, TX). MJF465, a triple *E. coli* mutant (*mscL*<sup>-</sup>, *mscS*<sup>-</sup>, *mscK*<sup>-</sup>) (22), used in our work as a host strain was kindly provided by Dr. Ian Booth (University of Aberdeen, Scotland). The MscS S95C/I97C double mutant was generated with a single pair of complementary primers using a QuikChange mutagenesis kit (Stratagene, La Jolla, CA) and verified using automated sequencing.

### Preparation of membrane vesicles

The PB111 construct containing MscS-his<sub>6</sub> was transformed and expressed in MJF465 cells (22). Cells were grown from overnight culture in 800 ml Luria-Bertani medium at 37°C to an OD<sub>600</sub> of 0.6 and induced with 0.8 mM isopropyl- $\beta$ -D-thiogalactopyranoside for 1 h. Cells were collected by centrifugation. The cell-pellet was washed with 50 ml of 50 mM potassium phosphate buffer pH 8 containing 5 mM MgCl<sub>2</sub> and resuspended in the same buffer. The suspension was passed twice through a French press at 1.1 kbar. Unbroken cells were removed by low-speed centrifugation and membrane vesicles were collected by ultracentrifugation in a Ti60 rotor (45k rpm, 45 min, 4°C), resulting in ~0.6 g of cell membranes (wet weight). Membrane pellets were stored at -80°C until either being resuspended in 50 mM phosphate buffer pH 8 or used for the purification of MscS-his<sub>6</sub>.

### Purification of MscS-his<sub>6</sub>

His-tagged MscS was purified essentially as in Sukharev (23). An amount of 0.6 g of membrane pellet was dissolved in 8 ml of 50 mM potassium phosphate buffer pH 8, 300 mM NaCl, 20 mM imidazole, and 3% (w/v) octylglucoside. This solution was cleared from insoluble particles by ultracentrifugation (45,000 rpm, 45 min, 4°C). The resulting solution was incubated with 0.5 ml Ni<sup>2+</sup> nitrilotriacetic acid slurry on ice for 1 h. The slurry was poured into a column and eluted by gravity. The gel bed was washed with 10 volumes of 300 mM NaCl, 50 mM potassium phosphate buffer pH 8, 20 mM imidazole, and 1% (w/v) octylglucoside. Elution was performed stepwise with buffers containing 50, 75, and 200 mM imidazole, using two gel-bed volumes for each step. Aliquots were run on an 11% SDS-PAGE gel and stained with Coomassie G-250. Fractions containing purified MscS were pooled and supplemented with 0.1% (w/v) Triton X-100. The protein solution was stored at 4°C.

### TFE-induced dissociation of MscS detected by LDS-PAGE

Twenty-microliter samples of either MscS (0.3 mg/ml) or a membrane preparation from MJF465 cells containing roughly 4 mg/ml total protein were added to solutions of TFE in water for a total volume of 30  $\mu$ l. The samples were incubated at ambient temperature for 1 h. Samples were cooled on ice before addition of 7.5  $\mu$ l ice-cold LDS-PAGE gel loading buffer. Samples were run on either 9.5% continuous or 8–18% gradient LDS-PAGE gels. In several experiments, TFE-exposed membrane vesicles were spun down and the TFE-containing buffer was carefully removed before dissolution in LDS.

To facilitate detection of oligomeric MscS, electrophoresis was performed at low temperature. Precipitation of dodecyl sulfate was prevented

by replacing sodium dodecyl sulfate with lithium dodecyl sulfate in the gels and buffers. Otherwise, the gels and buffers were identical to those commonly used in SDS-PAGE. Electrophoresis setups, gels, and buffers were chilled before use and cooled continuously throughout each run. Gels were run at 120 V until the blue dye-front reached the edge of the gel. Gels were stained with Coomassie Brilliant Blue G-250 in the case of purified protein or subjected to Western-blotting with anti-his<sub>6</sub>-COOH antibodies in the case of inner membrane vesicles. Precision Plus All-Blue protein standards were from BioRad Laboratories.

## Electrophysiology

Patch-clamp recordings of MscS were performed using bacterial strains, equipment, and general techniques as previously described (26). Briefly, PB111, a plasmid construct containing MscS with a C-terminal his<sub>6</sub> tag, was transformed and expressed in MJF465 strain (22). Voltage-clamp recordings were taken at +30 mV (as measured in the pipette) from excised membrane patches of giant *Escherichia coli* spheroplasts. Patches and MscS activity were stimulated by reproducible ramps and pulses of negative pressure applied with a high-speed pressure-clamp apparatus HSPC-1 (ALA Scientific, Westbury, NY). Recording was conducted in symmetrical potassium buffer (200 mM KCl, 90 mM MgCl<sub>2</sub>, 10 mM CaCl<sub>2</sub>, and 5 mM HEPES titrated to pH 7.4 with KOH). TFE solutions were created by adding 99+% TFE (Sigma, St. Louis, MO) to the recording buffer for final concentrations of 0.5, 1.0, 2.0, 3.0, and 5.0 vol %. TFE solutions were made fresh before each experiment and solutions older than 3 h were discarded.

Membrane patches were exposed to TFE from the cytoplasmic (bath) or periplasmic (pipette) faces. Exposure to TFE from the bath occurred after establishment of a gigaOhm seal and patch excision. Recording buffer in the bath chamber (~4 ml) was replaced with three chamber volumes of TFE solution through perfusion. The total time of perfusion was 3 min, after which the system was allowed to rest for an additional 3 min before stimulation. After cytoplasmic exposure, TFE could be “washed out” using the same perfusion technique with recording buffer replacing the TFE solution. Exposure to TFE from the pipette was accomplished by filling the electrode with TFE solution (1–5 vol %) behind a 3–5 mm plug of pipette solution with 300 mM sucrose to delay the onset of exposure. This diffusion-limited delay (2–10 min) provided time to take control measurements.

## Data collection and analysis

Axon pClamp 9.2 software (Axon Instruments, Foster City, CA) was employed to record integral or single-channel current with a bandwidth of 5–10 kHz at a sampling rate of 30 kHz. The pClamp software was also used to control the pressure application via output commands to the pressure clamp in episodic stimulation mode. Two-channel recordings of current and pressure versus time were then analyzed with Axon Clampfit 9.2. The maximal current ( $G_{\max}$ ) achieved by the MscS population was calculated from traces as the average conductance after the pressure ramp reached its plateau. The midpoint pressure of activation ( $p_{1/2}$ ) was identified as the pressure at which the MscS population reached 1/2  $G_{\max}$ . Fitting of the inactivation and recovery kinetics was also performed in Clampfit using built-in fit protocols. A standard exponential function with one or two terms was employed with a Levenberg-Marquardt search method.

## Hydrophobicity analysis of MscS surfaces

The crystal structure of MscS (1MXM.pdb) (27) was used for mapping the hydrophobic and hydrophilic areas on the solvent-accessible surfaces of the entire protein. Estimations of the atomic solvent-exposed areas were performed using the web-based GETAREA program (31) with a probe radius of 1.4 Å. The hydration energy was computed as the product of the exposed area for each individual atom and the corresponding atomic

solvation energy parameter of Eisenberg (32). Hydration energies per amino-acid residue were introduced into the PDB structure file using the PDBAN program custom written in MatLab (The MathWorks, Natick, MA). The solvation energy density was mapped on the MscS solvent-accessible surface and visualized with color-code using VMD (32,33).

## RESULTS

### TFE-induced dissociation of MscS oligomers

To assess the stability of MscS oligomers, the protein, either as a membrane preparation containing MscS-his<sub>6</sub> or in purified, detergent-solubilized form, was incubated with varying concentrations of TFE before separation by LDS-PAGE. To assign the multimeric state of the gel-separated complexes, we attempted two sets of molecular weight markers. The first set was a commercial Precision Blue set (Bio-Rad) consisting of fully denatured soluble proteins (left side on all gels). As a second set we utilized disulfide-crosslinked subunits of the MscS S95C/I97C double cysteine mutant that formed ladders of products ranging from monomers to heptamers under nonreducing conditions (*right side*, Fig. 1 A).

Electrophoresis on *E. coli* membranes overexpressing MscS-his<sub>6</sub> was performed using a gradient-gel to allow for adequate resolution in the high-molecular-weight region. LDS-PAGE followed by Western-blotting with anti-his<sub>6</sub>-C-term antibodies revealed three bands (Fig. 1 A, lane 1). According to the soluble marker scale (*left side*), the upper band ran at 300 kDa, the second, most intensive band appeared to be close to 250 kDa, and one lightly stained band at 25 kDa. Boiling the sample before electrophoresis produced a single band of monomeric MscS at 25 kDa (Fig. 1 A, lane 2).

Since the mobility of membrane proteins in dodecyl-sulfate gels may deviate considerably from that of soluble proteins, electrophoresis standards made of soluble proteins may not provide accurate estimations of molecular weight. Therefore we utilized a double-cysteine mutant of MscS, which spontaneously cross-links under ambient atmospheric oxygen, to compare the migration patterns of known covalent homo-oligomers of MscS and assess the oligomeric state of the observed high-molecular-weight bands in unboiled MscS samples. Fig. 1 A, lane 3, shows that the covalent oligomers migrate mainly as two bands at the same location as the regular MscS oligomers. When the double-cysteine mutant was boiled before loading, a ladder of denatured, covalent oligomers was observed (Fig. 1 A, lane 4). The exact sequence-based molecular weights for these bands are presented in parentheses on the right side of the gel. The difference between the two scales shows that in an 8–18% polyacrylamide gel, denatured MscS monomers and dimers run slightly faster than soluble proteins of similar sizes, whereas larger cross-links (4×–7×) migrate slower. As expected, boiling the double-cysteine mutant in the presence of DTT caused most of the higher MW bands to disappear and the monomer band to increase in intensity (Fig. 1 A, lane 5).

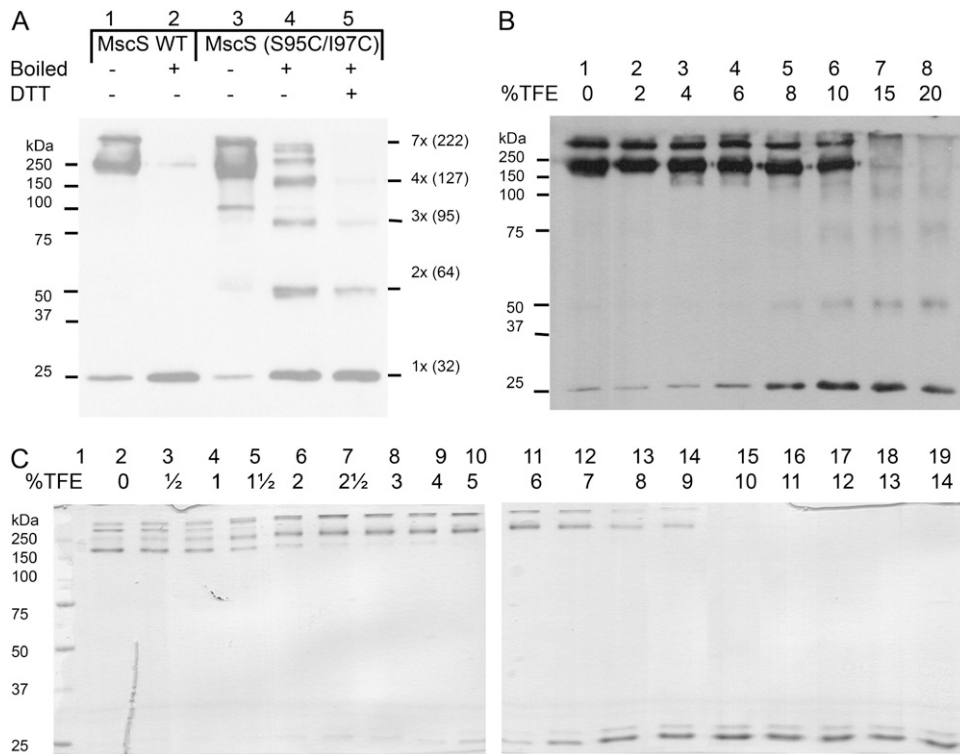


**FIGURE 1** (A) Migration of MscS-<sub>6</sub>his and MscS-his<sub>6</sub> S95C/I97C in *E. coli* membranes as visualized on anti-his<sub>6</sub>-C-term Western-blot of an 8–18% LDS-PAGE gradient gel. Lane 1 contains membrane vesicles of MJF465 overexpressing MscS-his<sub>6</sub>. The sample was kept on ice after exposure to LDS gel loading buffer. Lane 2 shows the same sample after boiling for 5 min upon addition of LDS-PAGE gel loading buffer. Lane 3 was loaded with membranes of MJF465 overexpressing MscS-his<sub>6</sub> S95C/I97C. The sample has undergone the same treatment as that in lane 1. Lanes 4 and 5 show MscS-his<sub>6</sub> S95C/I97C loaded in membrane vesicles after boiling without and with 14 +mM of DTT, respectively. Positions of soluble molecular weight markers indicated on the left are used to provisionally designate the band positions. Marker positions based on disulfide-crosslinked MscS subunits providing better estimations for actual molecular weights are shown on the right with calculated molecular weights in parentheses (kDa). For reasons of legibility the pentamer and hexamer have been omitted. (B) TFE-induced dissociation

of MscS-6his in *E. coli* membrane vesicles as visualized by anti-his<sub>6</sub>-C-term Western blotting on a continuous 9.5% LDS-PAGE gel. Lanes 1–8 were loaded with membrane vesicles of MJF465 overexpressing MscS-his<sub>6</sub> that were incubated for 1 h at room temperature with the indicated percentages of TFE. Densitometry indicated that the total protein intensity in lane 8 is reduced to a third compared to lane 1, presumably due to monomer aggregation. A molecular weight marker is shown on the left. (C) TFE-induced dissociation of purified oligomeric MscS-6his in 1% (w:v) octylglucoside and 0.1% w:v TX100 on a continuous 9.5% LDS-PAGE gel. Aliquots of purified MscS-his<sub>6</sub> protein solution (0.3 mg/ml) were incubated with the indicated percentages of TFE for 1 h at room temperature and analyzed by LDS-PAGE. The gel was stained with Coomassie Brilliant Blue G-250.

We presume that the positions of covalently cross-linked oligomers of MscS itself (Fig. 1 A, lane 4) give more reliable estimations of MW than the soluble protein standards. Migration of the bands in this sample suggest that the upper band in lanes 1 and 3 represent intact heptamers, whereas the most intensively stained band near the 250 kDa soluble marker arises from tetramers of MscS subunits that partially retain tertiary structure. Therefore, to interpret these data, we propose assignment of molecular weights according to the disulfide-cross-linked multimers of MscS (Fig. 1 A, right). Using this interpretation, heptameric MscS is observed to run at a higher molecular weight than its covalently-linked, denatured heptamer. This result may seem surprising because compactly folded (nondenatured) proteins usually migrate in gels faster than their denatured counterparts. However, native MscS contains a bulky cage-like C-terminal domain, a feature that may cause the native form to migrate slower than the denatured protein.

To test whether MscS oligomers can be dissociated by exposure to TFE, membrane vesicles of a strain overexpressing MscS-his<sub>6</sub> were incubated with TFE for 1 h at ambient temperature, before being subjected to electrophoresis on continuous LDS-PAGE gels. Fig. 1 B shows that the

upper bands disappear from the gel after exposure to TFE while a monomeric band appears. Both oligomeric forms of the protein disappear at concentrations of TFE >10 vol %, although some signal remains at high molecular weight. This residual signal may be the result of MscS aggregation. Aggregation may also explain the relatively low intensity of the monomeric band since such an effect was observed previously for KcsA upon exposure to high concentrations of TFE (17). To verify that the observed decomposition of MscS complexes to monomers is specifically due to the presence of TFE, but not a result of the combined action of TFE and LDS, in a separate experiment we pelleted the TFE-exposed membranes and carefully removed the TFE-containing buffer before adding the LDS sample buffer. This procedure led to a dilution of the residual TFE by at least 10-times. The resultant pattern of bands in the gel was similar to that in Fig. 1 B showing a breakdown between 10 and 15 vol % TFE (data not shown). This suggests that TFE present around and inside the membrane is, by itself, capable of disrupting intersubunit interactions in MscS.

To establish whether the effect of TFE on the MscS-his<sub>6</sub> protein is dependent on the membrane context or it is an intrinsic property of the protein, preparations of purified

protein in octylglucoside were also subjected to TFE-induced dissociation. The addition of minor amounts of Triton X-100 (0.1% w/v) was found to improve the stability of the purified protein in LDS-PAGE. Under these conditions, purified MscS migrates as a group of four bands with the most dense one, presumably tetrameric, migrating as the lower oligomer band seen in the membrane preparation gel (Fig. 1 C, lane 1). Exposure of MscS to 2–6 vol % TFE causes some bands to disappear, while simultaneously increasing the intensity of the heptameric and likely pentameric bands (Fig. 1 C, lanes 6–11). Apparently, even low amounts of TFE are sensed by the protein, causing it to migrate more slowly, likely due to the effect of “swelling” of hydrophobic cavities and voids (34).

Increasing the TFE concentration to 10 vol % causes complete dissociation of MscS into monomers (Fig. 1 C, lane 15). In this case no significant loss of protein was observed. The concentration of TFE resulting in a complete dissociation of MscS in detergent micelles was slightly lower than that required to achieve the same result in native membranes. Nevertheless, these concentrations are similar, which suggests that TFE-induced dissociation is an intrinsic property of the protein, which may be slightly stabilized by the lipid bilayer as compared to detergent micelles. The ability to dissociate MscS is not exclusive to TFE, as other alcohols such as 1,1,1,3,3,3-hexafluoroisopropanol produce the same effect on MscS albeit at lower concentrations (data not shown).

### TFE effects on MscS activation by pressure ramps

As was shown previously (26), MscS steeply activates in response to 1 s duration, linear ramps of negative pressure followed by a plateau (Fig. 2). After reaching saturating pressure, MscS stays open for the duration of pressure stimulus. In control experiments with a large number of channels per patch (50 or more), maximal current ( $G_{\max}$ ) of the population reproduced itself within 10%. Using a typical size of patch pipettes, the midpoint pressure of activation ( $p_{1/2}$ ) varied in the range between 120 and 170 mm Hg; however, within each patch, sequential sweeps grouped tightly around a single midpoint with <2% deviation around the mean (26).

We tested the effects of TFE on MscS function in a range of concentrations between 0.5 and 5 vol %. Lower concentrations had no observable effect, whereas higher concentrations of TFE mechanically destabilized patches, thus precluding reliable measurements. Patches exposed to 1 vol % TFE from the pipette (periplasmic side of the membrane) displayed a slight (~5 mm Hg) leftward shift of the dose-response curves without any significant effect on  $G_{\max}$ . The time for development of the leftward shift at this concentration was long (>1 h). When the concentration of TFE was increased to 3–5 vol %, larger decreases in  $p_{1/2}$  (leftward shifts) of ~20 mm Hg were observed. The ratio of midpoints for 5 vol % TFE in the pipette, as compared to control, was

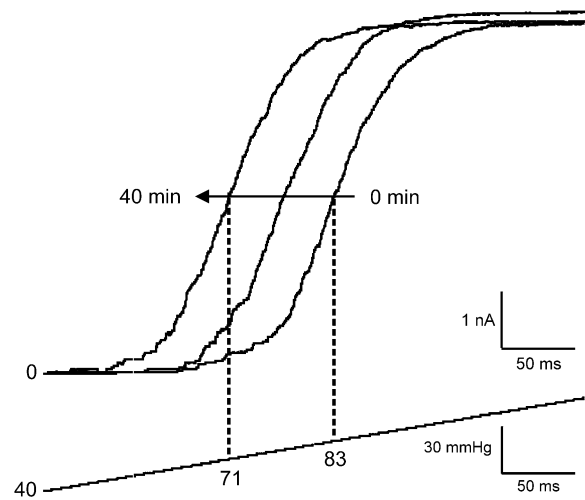


FIGURE 2 Dose-response curves of MscS measured with TFE in the pipette. The tip of the pipette was first filled ~5 mm with recording solution plus sucrose without TFE. The pipette was then backfilled with recording solution plus 5 vol % TFE. Shown are three traces taken immediately after patch formation before TFE could diffuse into the tip (right), after 20 (middle) and after 45 min (left) of incubation. The bottom trace shows the linear ramp of the pressure gradient and the scale of the midpoint shift upon TFE application.

$0.93 \pm 0.04$  ( $n = 3$ ). These concentration-dependent shifts occurred reproducibly in the course of 45-min incubations (Fig. 2). During most experiments  $G_{\max}$ , and the corresponding number of active channels in the population, remained essentially constant, falling well within previously established levels of control variability (8–10%).

Perfusion of TFE from the bath (cytoplasmic side of the membrane) even at low concentrations (0.5–2 vol %) invariably shifted  $p_{1/2}$  to the right by ~10–40 mm Hg (Fig. 3, A–C). The peak ratio of midpoints for 2 vol % TFE in the bath, relative to control, was  $1.13 \pm 0.08$  ( $n = 4$ ). The presence of TFE in the bath appears to make the midpoint less stable from trace to trace when compared to controls. In all bath-perfusion experiments the initial and fastest midpoint movement was always to the right. However, in very long experiments (>2 h),  $p_{1/2}$  and  $G_{\max}$  were observed to slowly return to the untreated level. We subsequently found that TFE is very volatile and evaporates from a 35 mm Petri dish filled with 5 vol % TFE at a rate of ~2  $\mu\text{l}/\text{min}$ . In the course of 100 min its concentration is thus expected to drop by 80–90%. It was observed that the return of  $p_{1/2}$  and  $G_{\max}$  to control values occurs roughly within this time frame.

TFE presented to the cytoplasmic side reproducibly decreased  $G_{\max}$  of the MscS population as measured by standard 1 s ramps of pressure. A measurable decline (>10%) was observed at 0.5 vol %, with nearly complete silencing of the entire population by a 5 vol % solution (Fig. 3 C). The concentration of TFE that causes 50% inactivation appears to fall between 0.7 and 1 vol %, due to natural variability in patches and spheroplast preparations. This

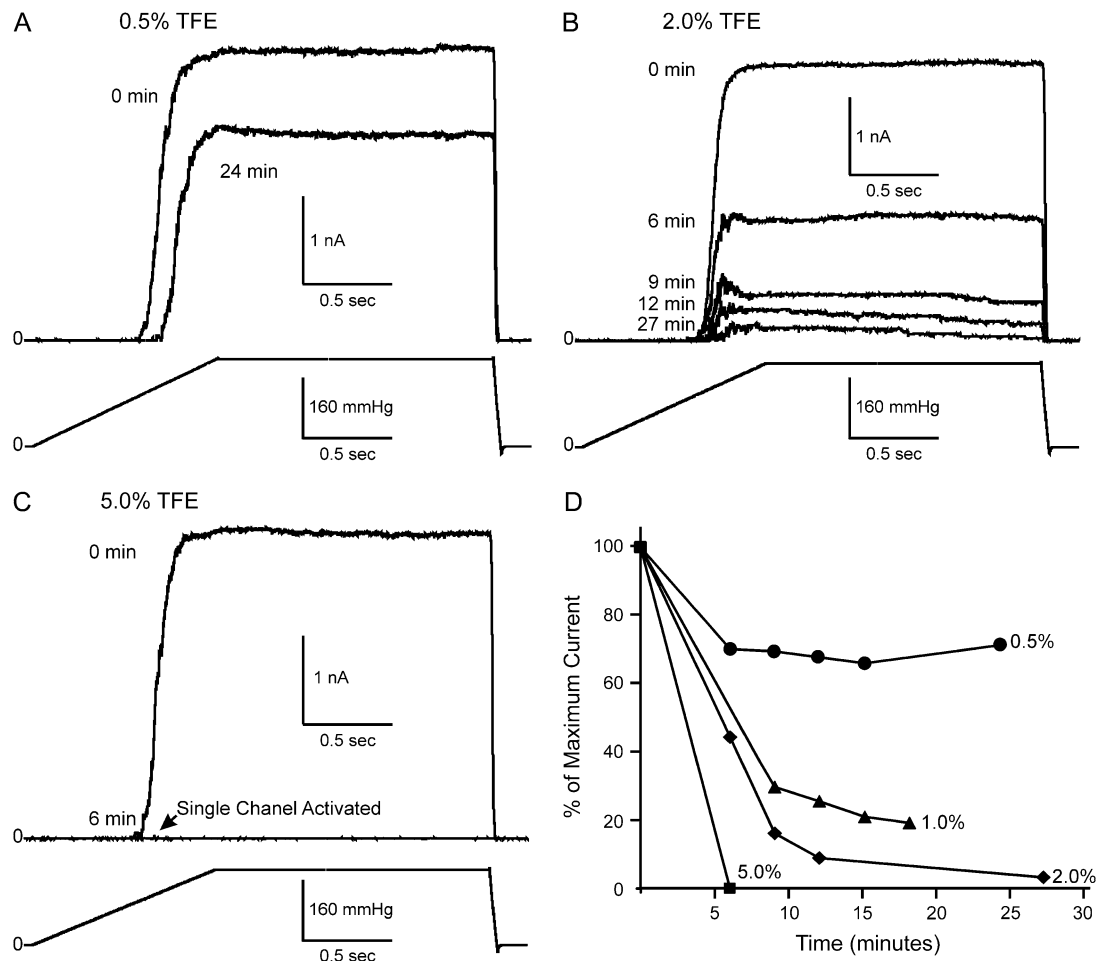


FIGURE 3 Effects of TFE on dose-response curves of MscS measured in excised inside-out patches. TFE was applied to the cytoplasmic side (bath). After equilibration, 1 s linear ramps of negative pressure reaching saturating level followed by a 1.5 s plateau were applied in 3 min intervals. Population responses to 0.5, 2.0, and 5.0 vol % TFE are presented in panels A–C, respectively. A right shift of the activation curve (midpoint change from 156 to 180 mm Hg) in the presence of TFE is seen in panel A. Time course of current decline in the traces taken at 6–27 min time points (B) indicate MscS inactivation at saturating pressures in the presence of TFE, not observed in controls. The midpoints for these traces are 161 (control), 161 (6 min), 163 (9 min), 166 (12 min), and 179 (27 min) mm Hg. Arrow in panel C points to a single channel transiently activated after exposure to 5 vol % TFE followed by complete inactivation. Plot of maximal current achieved by channel population as a percentage of the maximal current before TFE addition (D). The curves in all panels represent inward currents at +30 mV pipette potential.

concentration-dependent process of silencing was not instant but developed within the course of 7–20 min (Fig. 3 D).

To verify that the decrease in  $G_{\max}$  was not due to a drastic change in single-channel conductance, we performed measurements of I-V curves in the presence and absence of TFE (Fig. 4 A). The single-channel conductance in the presence of 3 vol % TFE in the bath was essentially the same as in control except for a small deviation at strongly depolarizing voltages (–80 mV pipette) where the open state current becomes noisy due to the increased presence of subconducting states. The pipette electrode potential has been tested independently in the presence of 5 vol % TFE, and we observed no systematic deviation  $> \pm 1$  mV.

To further demonstrate that the observed reduction of  $G_{\max}$  in the presence of TFE was not caused by the right shift of the activation curve, we stimulated the TFE-silenced

population with a double-ramp protocol (Fig. 4 B). Before TFE application, the patch was tested with a saturating ramp of pressure followed by a plateau evoking a  $\sim 4.09$  nA current. After exposure to 2 vol % TFE for 15 min, the current stimulated by the same ramp fell to 0.44 nA. Additional pressure applied in the form of a second ramp to a higher plateau did not evoke any extra activity. The inset in Fig. 4 B shows expanded segments of these traces to illustrate again that the single-channel amplitudes before and after TFE addition are identical.

TFE-induced silencing was also found to be reversible. A washout of TFE with recording solution returned 80–100% of the inactivated population back to the active state even after complete silencing with the highest concentration of TFE tested (5 vol %). On washout,  $p_{1/2}$  typically shifted back to the left, returning to a pressure close to the control (before

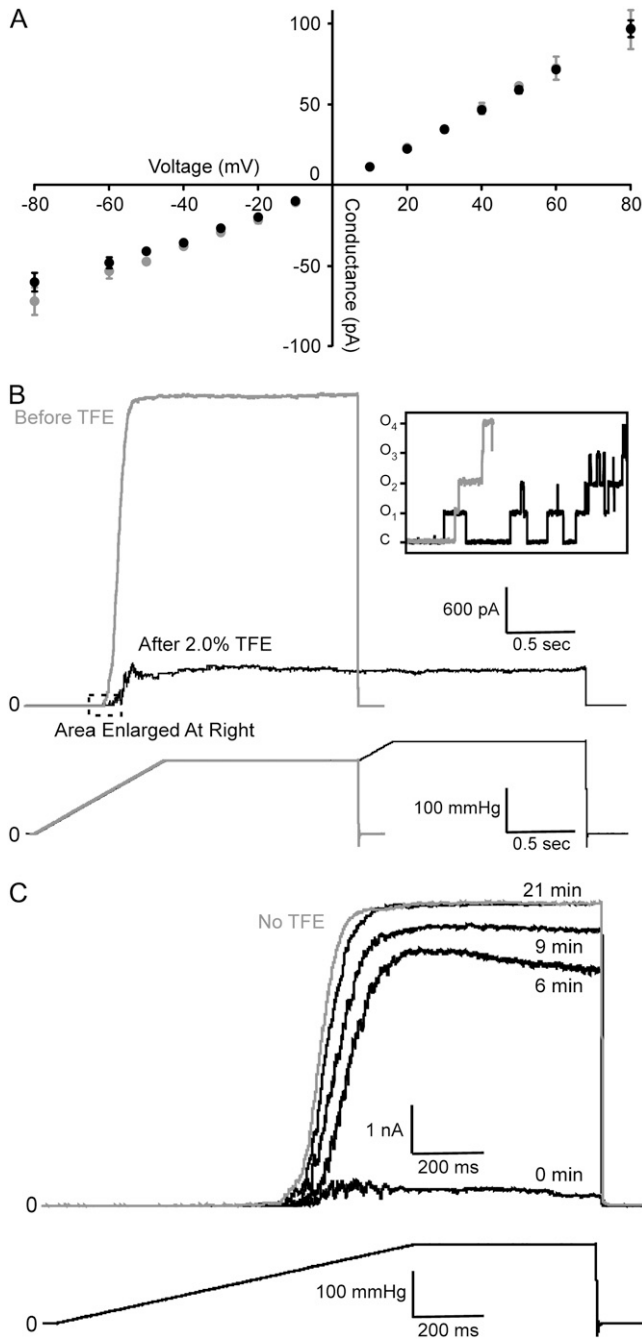


**FIGURE 4** Experiments illustrating the nature of  $G_{\max}$  reduction in the presence of TFE. (A) Current-to-voltage relationships for MscS in control (shaded circles) and in the presence of 3 vol % TFE (solid). (B) Effect of additional pressure on a TFE-silenced MscS population. The shaded trace represents the 4.09 nA MscS current in response to a 1 s pressure ramp to 160 mm Hg followed by a 1.5 s plateau, recorded before TFE application. The solid trace shows the 0.44 nA response of the same patch 15 min after application of 2 vol % TFE in the bath. The pressure protocol was extended by an additional ramp reaching higher pressure (200 mm Hg), which did not produce any additional activity indicating that the active part of channel population is fully saturated by the first stimulus, whereas the rest is in an inactivated state. (C) The kinetics of recovery after TFE washout. The shaded trace represents the response of a freshly excised patch without TFE, whereas the lower trace (0 min) shows residual current after a 20

min exposure to 3 vol % TFE. A washout resulted in a gradual return of the population current to a pre-TFE level, within ~20 min. Shifting of the midpoint to the left occurs concomitantly with the recovery. The mid-point values are 131 (6 min), 127 (9 min), 122 (21 min), and 119 mm Hg in control.

### Stimulation by fast ramps and pulses: effects of TFE on inactivation and recovery

To address the nature of the TFE-silenced state of MscS, we investigated population responses to pressure ramps applied with different speeds as well as responses to steeply applied stimuli (pulses). Previously published data (26) demonstrated that the MscS population responds fully to fast (<3 s) ramps of saturating pressure, but with slower ramps (10–90 s), only a fraction of population reaches the conductive state. The part of the population that does not conduct appears to inactivate while the ramp passes slowly through a range of intermediate pressures. Fig. 5 A depicts MscS responses to short pressure ramps in the presence and absence of TFE. The set of control experiments without TFE (shaded) demonstrates that 0.1, 0.5, 1, and 2 s ramps evoke essentially the same maximal current from the MscS population as our fastest (hardware-limited) test pressure pulses (10 ms rise time, 250 ms duration). Upon addition of 3 vol % TFE to the same patch (bath perfusion), a 2 s ramp was observed to evoke <8% of the original  $G_{\max}$ . Progressively faster stimuli were found to activate larger fractions of channels population. A declining slope of  $G_{\max}$  during the pressure plateau at the end of each ramp reveals an increased propensity to inactivation. We know from the previous studies (22,25,26) that MscS displays the tendency to inactivate when subjected to intermediate pressure stimuli (above the threshold and below saturation). In the inactivated state, the channel does not conduct and is no longer responsive to even saturating stimuli. Traces recorded from the same patch with rectangular steps of subsaturating pressure (Fig. 5 B) show that indeed, 3 vol % TFE increases the rate of inactivation ~10 times. These data presented in Fig. 5 reveal that MscS channels do not inactivate spontaneously from their resting state upon exposure to TFE as sharply applied stimuli can elicit activation of the channel population. At subsaturating pressures, TFE speeds up the process of inactivation, which appears to be the reason for the decreased fraction of active channels at slower rates of stimulus application.

Recovery of the MscS population from the inactivated to the resting state was also found to be influenced by TFE. Previous experiments revealed that this process is kinetically

min exposure to 3 vol % TFE. A washout resulted in a gradual return of the population current to a pre-TFE level, within ~20 min. Shifting of the midpoint to the left occurs concomitantly with the recovery. The mid-point values are 131 (6 min), 127 (9 min), 122 (21 min), and 119 mm Hg in control.

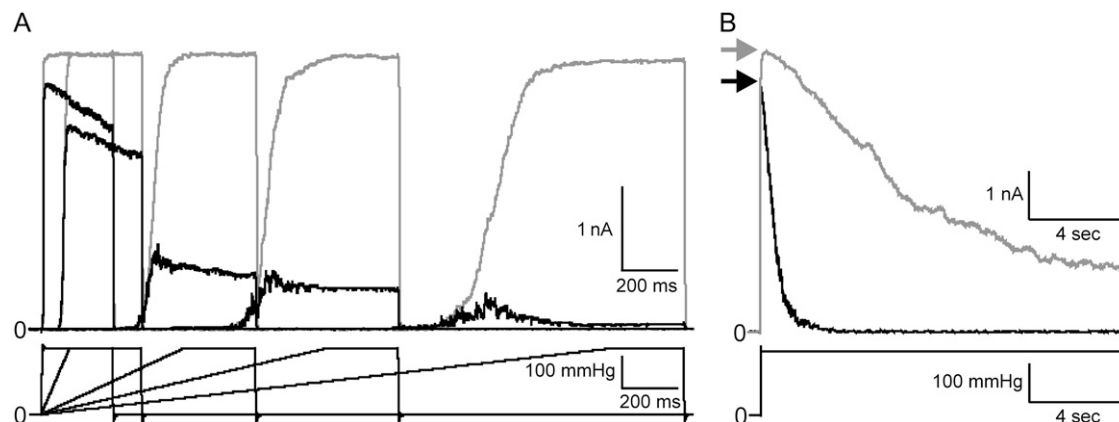


FIGURE 5 MscS responses to ramps and pulses. (A) Increasing the speed of linear ramps from zero to a saturating pressure (200 mm Hg) evokes progressively larger current in patches treated with 3 vol % TFE on the cytoplasmic side (*solid traces*). Ramp speed was changed after stabilization of  $G_{\max}$  under the 1 s stimulus, with each subsequent stimulus separated by 3 min intervals. A control set of traces taken before TFE perfusion (*shaded*) shows no difference in the maximal current at this range of ramp speeds. (B) Responses to a step of subsaturating pressure (160 mm Hg) recorded on the same patch before (*shaded*) and after TFE perfusion (*solid*). Arrowheads indicate the maximal level of conductance upon application of the pressure stimulus. The current decay time ( $\tau_i$ ) decreased from 2.8 s in control to 0.25 s, with TFE illustrating a higher rate of inactivation.

complex, with full recovery taking  $\sim 3$  min under zero applied pressure (26). A typical response of WT MscS to an intermediate stimulus, followed by a series of short saturating stimuli designed to test the kinetics of recovery, is shown in Fig. 6, A and B. An applied 25 s step of subsaturating pressure initially opens  $\sim 95\%$  of channel population. This spike of channel activity decays almost monoexponentially with a characteristic inactivation time ( $\tau_i$ ). The  $\tau_i$  in MscS is not constant and becomes longer with increasing amplitude of the intermediate pressure stimulus (26). By the end of a 25 s intermediate stimulus, the current approaches the baseline signifying that the entire population is now in a non-conductive state. A short (0.25 s) test pulse of saturating pressure immediately after the 30 s step (Fig. 6 B) reveals that most of the population is now unresponsive to the stimulus with the exception of a small variable fraction ( $\sim 0$ –15%) that still responds to the saturating pressure. A train of test pulses spaced at 1, 10, 30, and 60 s after the intermediate pulse illustrates the kinetics of recovery. Recovery appears to be a multiexponential process with at least two components ( $\tau_{1r}$  and  $\tau_{2r}$ ). We observed a relatively fast component in the beginning ( $\tau_{1r} = 1.8$  s,  $\sim 85$ –90%  $G_{\max}$ ), followed by a much slower recovery to the initial  $G_{\max}$  ( $\tau_{2r} = 18.9$  s). Although the control curve presented here is fit relatively well with two exponents, a third component with a longer characteristic time but smaller contribution may exist.

After perfusion of 0.5 vol % TFE on the cytoplasmic side,  $G_{\max}$  measured with a 1 s ramp stabilized at 75–90% of its initial level. Experiments were carried out only after stabilization of  $G_{\max}$ . Even at this low concentration of TFE, inactivation after a stimulus near  $p_{1/2}$  was on average  $2.6 \pm 0.8$  times faster (mean  $\pm$  SD,  $n = 6$ ).

TFE markedly slows down the process of recovery from the inactivated state. Fig. 5 C shows the normalized conduc-

tance of the channel population as a function of time after the intermediate stimulus. The recovery curve from the TFE treated population was fit with a single exponent producing a characteristic  $\tau_r$  of 10.6 s. The recovery data for the TFE-treated population was fit better with one exponent than with two. This suggests a delay in the onset of the second, longer recovery component, observed in the control. For comparison, the initial part of the control recovery curve was fit with a single exponent producing characteristic time of  $\tau_r$  of 2.4 s. The fast stage of recovery of the TFE-treated population to 80%  $G_{\max}$  was therefore  $4.2 \pm 0.4$  times slower than untreated control ( $n = 7$ ) (Fig. 6 C).

## DISCUSSION

The results described above depict two types of events taking place at different concentrations of TFE in the aqueous solution. At lower TFE concentrations (1–5 vol %), we observe a dramatic effect on the kinetics of channel redistribution between the functional states, whereas at higher concentrations (10–15 vol %) MscS channels dissociate into monomeric form. It appears that the nature of these two effects is qualitatively the same and rests primarily on the capability of TFE to partition into membranes or detergent micelles and to perturb buried interhelical contacts.

Previous work (21) identified MscS as part of an oligomeric protein complex that survives solubilization in SDS at room temperature but becomes dissociated by TFE. In this study, we showed that MscS forms stable oligomers in cold, ionic-detergent (LDS) gel electrophoresis. Previously, oligomeric MscS could only be visualized by using Blue-Native PAGE (35).

Exposure of the protein in membrane vesicles to 15 vol % TFE was found to result in dissociation of oligomeric MscS

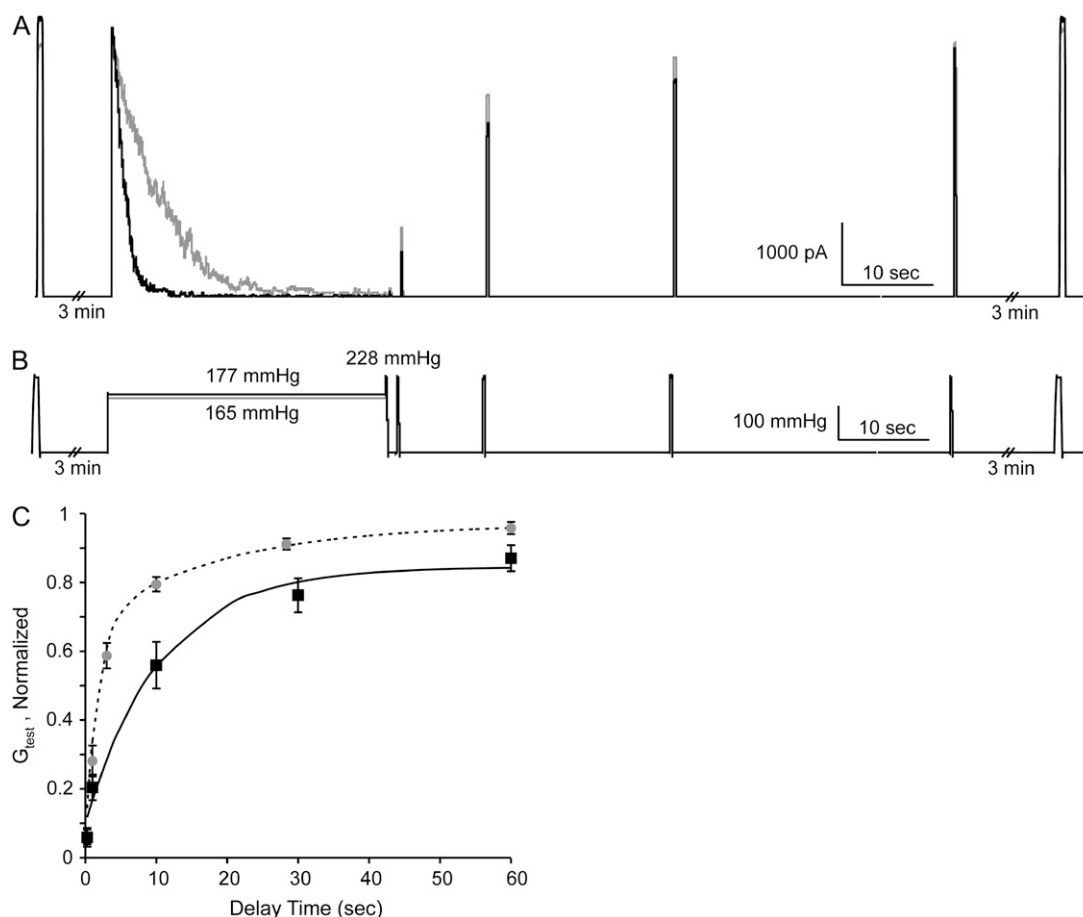


FIGURE 6 Effect of TFE on the rate of MscS inactivation and recovery. Inside-out patches containing  $\sim 125$  active MscS channels were subjected to a pressure step of 25 s duration, during which the channels transiently open and display inactivation kinetics. The pressure stimulus is followed by a train of 0.25 s test pulses, which permit our monitoring the time course of recovery (A). A single test pulse of saturating pressure (preceding the stimulus by 3 min) indicates the maximal current attainable in the patch ( $G_{max}$ ). (B) Representative current traces recorded before (shaded) and after (solid) perfusion of 0.5 vol % TFE in the bath. (C) The time course of recovery before (shaded circles) and after perfusion of 0.5 vol % TFE. The recovery kinetics was fit with one and two exponents, with and without TFE, respectively.

into its monomeric subunits. A similar behavior was observed at 10 vol % for the purified, detergent-stabilized protein. This effect of TFE on MscS could potentially arise from two mechanisms. First, TFE could act via the lipid-phase by changing the packing properties of the bilayer as was observed for KcsA (17). Second, TFE may dissociate protein complexes by simply weakening the contacts between the subunits and/or associated lipids. Since we observe dissociation in MscS at approximately the same concentration, both in the context of the *E. coli* inner membrane and in detergent micelles, it seems likely that TFE works mainly by the latter mechanism, although the complexes are slightly more resistant to TFE when surrounded by the native lipid bilayer. Removal of free TFE from the system before membrane solubilization in LDS does not change the outcome, suggesting that TFE by itself critically compromises intersubunit interactions already in the membrane, and the dissociation of MscS does not appear to be a result of cooperative action between TFE and the detergent.

The existing data indicates a clear difference between TFE's effects on soluble and membrane-embedded proteins. The ability for TFE to stabilize helical conformations in peptides and accelerate protein folding has been explained by aggregation of TFE around the protein backbone, local exclusion of water from the competition for hydrogen bonds, and possibly by lowering the effective dielectric constant of the solvent (36). This mechanism is consistent with TFE's tendency to form microscopic clusters in aqueous solutions (1,9), partition into hydrophobic protein crevices (34), and promote desolvation of protein surfaces that normally form buried contacts (14,36). At the same concentrations (15–30 vol %) that stabilize soluble proteins, TFE completely disrupts KcsA and MscS as well as many other membrane complexes (17,21).

Soluble proteins are stabilized by the formation of a dehydrated core. They are held together by hydrophobic interactions as well as strong polar interactions in a largely nonaqueous environment. TFE does not interact strongly

with hydrophobic side chains (15), and thus does not unfold the hydrophobic core of a soluble protein until the concentration in the surrounding aqueous solution exceeds 50%. Membrane proteins, on the other hand, have an inverted design when compared to typical soluble proteins (37,38). They have water-filled cavities with hydrocarbon-exposed hydrophobic rims, and are stabilized by interactions with the surrounding lipids. The lipid bilayer could be considered a two-dimensional anisotropic solvent for membrane proteins where the lipids exist in a liquid crystalline state. Lipid tails are relatively large and do not easily intercalate between the helices thus preserving interhelical contacts. In contrast, TFE is small and thus capable of wedging between helices and separating them. Helical separation may be initiated primarily at the membrane boundaries where the TFE concentration is expected to be the highest.

In the transmembrane part of the MscS crystal structure solved by Bass and co-workers (27) (Fig. 7) only the central helices (TM3) form intersubunit contacts. The peripheral helices TM1 and TM2 do not form a continuous lipid-facing wall, but protrude outward at an angle, forming deep hydrophobic crevices. Given that tilting of individual transmembrane helices in the bilayer is energetically unfavorable (39,40), the absence of tilt-stabilizing helical contacts between the TM1-TM2 pairs suggests that this unusual angle could be a result of delipidation. Several independent MD simulations showed that when embedded in lipids, without tension, this structure quickly collapses (30,41). This sug-

gests that 1), the resting conformation should be more compact, consistent with the hypothesis proposed by Booth and co-workers, and supported by cross-linking studies (42,43); and 2), under certain conditions the peripheral helices can detach from the pore-lining TM3s, thus forming crevices. As shown by the color-coded map of the protein surface (Fig. 7 B), the crevices are largely hydrophobic and could be occupied by an apolar solvent such as TFE. Previous measurements of the adiabatic compressibility demonstrated an increase of protein (lactalbumin) volume in the presence of 10–20 vol % of TFE indicating induction of packing defects and preferential accumulation of the co-solvent in hydrophobic crevices (34). For membrane proteins, partitioning of TFE into the lipid would increase the chance of penetration into interhelical gaps and the crystal structure suggests where these gaps may form in MscS.

Based on the above considerations and previous work (26,42), our model of the MscS native resting state is schematically represented as a compact conformation with the TM1-TM2 pairs packed along the TM3s (Fig. 8 A). In the resting state, the TM1-TM2-TM3 interactions are strong enough to transmit mechanical forces from the lipid bilayer to the gate. Applied tension expands the entire barrel making it conductive (Fig. 8 B). A subsequent detachment of the pore-lining TM3 helices from the peripheral helices, accompanied by kink formation at Glycine-113, leads the channel into a tension-insensitive inactivated state (Fig. 8 C).

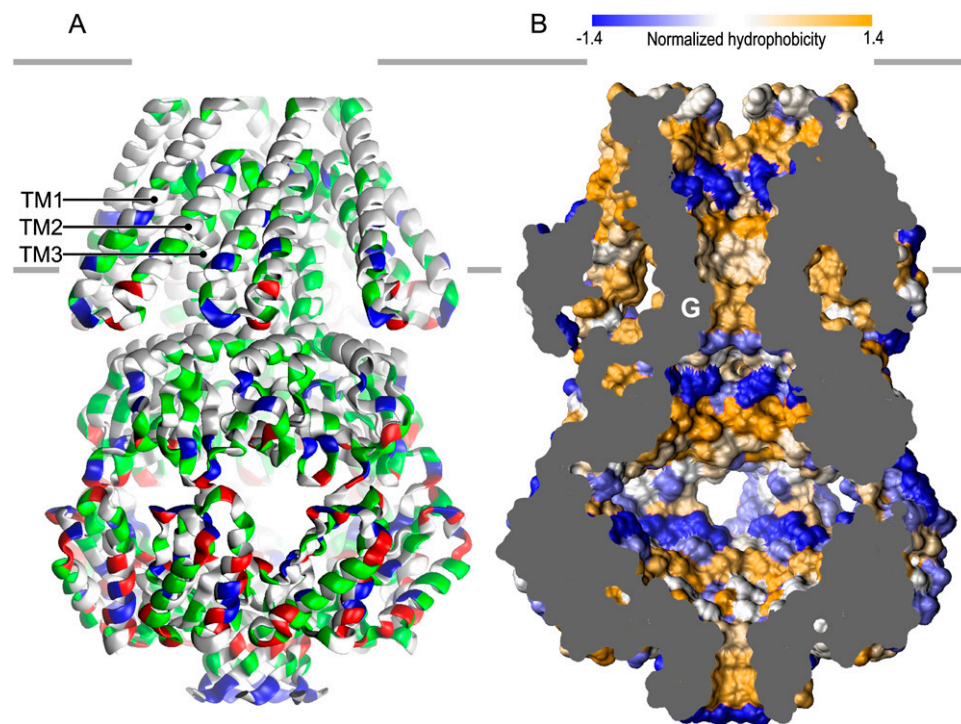


FIGURE 7 The crystal structure of MscS (A) (1MXM.pdb) and a vertical slice through the channel shown in a space-filled representation (B). The solvent-accessible surfaces were created with the probe of 1.4 Å in radius and colored according the normalized consensus hydrophobicity scale (32). The most hydrophobic areas (the pore constriction, TM2-TM3 crevices, and the distal parts of pore vestibules) are yellow and most hydrophilic regions (rings of charges in the vestibules and the equatorial part of the cytoplasmic cage) are blue. Computation and averaging of solvation parameters was performed using HISTAN (see Methods). The pore with the hydrophobic gate (denoted as G) is formed by the seven TM3 helices contributed from each subunit. Deep hydrophobic crevices separating the TM3 barrel from the peripheral TM1-TM2 helices might be a result of delipidation. In the crystal structure these crevices are likely filled by the detergent, whereas in our experiments, these spaces can potentially be occupied by TFE. It is thus possible that the peripheral helices in the TFE-induced inactivated state are

less tilted than in the crystal structure. The putative positions of membrane boundaries are shown by horizontal lines. The position of the outer boundary implies that 26 N-terminal residues missing from the crystal structure may form a periplasmic extension of the transmembrane domain.

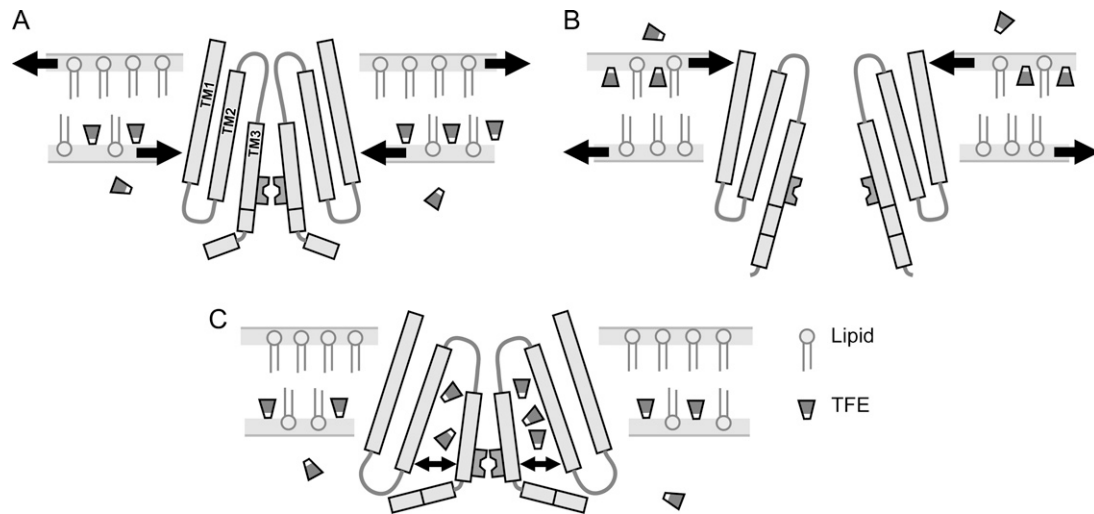


FIGURE 8 A schematic illustration of the hypothetical conformations of the transmembrane domain of MscS in the closed (A), open (B), and inactivated (C) states and the mechanism of TFE-induced perturbations. The gate of MscS is located at the cytoplasmic side and thus the channel is predicted to be more sensitive to increased tension in the inner leaflet. Intercalation of TFE in the inner leaflet (A) would create an extra lateral pressure shifting the equilibrium to the closed state. Addition of TFE to the periplasmic side expands the outer leaflet and produces tension in the inner leaflet, promoting opening (B). When present on the cytoplasmic side in sufficiently high concentration, under membrane tension TFE penetrates the crevices between the TM1-TM2 pair of helices and TM3 facilitating the transition to the inactivated state (C). The black arrows show the locations of TFE-induced tension/pressure components, which superimpose with the externally applied far-field tension used as a stimulus.

Why are the dose-response curves susceptible to perturbation by low concentrations of TFE, and how does TFE promote inactivation of MscS? It is likely that the membrane acts as an apolar reservoir attracting TFE. Although the exact partitioning coefficient of TFE between membranes and aqueous solutions has not yet been measured, it is known that  $\log P$  octanol/water is 0.41, indicating  $\sim 2.5$ -times higher preference for the bulk organic phase. Having an OH group with hydrogen-bonding capacity, TFE, like ethanol (44,45), may preferentially accumulate at the polar-apolar interface of the membrane, where its concentration could be higher than that in the bulk. Intercalation of TFE into the interfacial layer may additionally change the dipole and the surface components of the membrane boundary potential, thus perturbing lipid-lipid interactions and local interactions with proteins. At concentrations of 10 vol % and above, TFE perturbs phosphatidylcholine liposomes based on permeability tests. Inclusion of phosphatidylethanolamine was found to make the bilayer more resistant to permeabilization by TFE (17).

The partitioning of TFE is clearly reflected by measurable shifts in the MscS activation dose-response curves. These shifts are dependent on the membrane face (cytoplasmic or periplasmic) to which TFE is applied (Figs. 2 and 3). One possible mechanism for TFE action is illustrated in Fig. 8 combined with a schematic representation of the functional cycle of MscS. When adding TFE to the periplasmic face of the patch (pipette), TFE intercalates into the outer leaflet and increases its area. Because the two leaflets of the membrane are area-coupled by the common midplane, the expansion of

the outer leaflet of the membrane must create tension in the inner leaflet (46,47). Since the gate in MscS is located more toward the cytoplasm (27), channel activation is likely to be sensitive to tension in the inner leaflet (Fig. 8 B). Extra tension in the inner leaflet, created by TFE intercalation, should promote early activation of the MscS population. This was indeed the observed result, as addition of TFE to the periplasmic face caused a leftward-shift of the dose-response curves (Fig. 2). In contrast, when TFE is presented to the cytoplasmic face of the patch (bath perfusion), partitioning of TFE increases lateral pressure in the inner leaflet (Fig. 8 A), causing a right-shift of the activation curve (Fig. 3, A and B). Increased pressure caused by TFE intercalation partially negates the applied tension. The fact that the magnitude of the right-shift is not always stable suggests that TFE can, given sufficient time, redistribute between the leaflets thus dissipating the asymmetric area perturbation. This interpretation, however, needs to be taken with caution, as it has not been demonstrated that excised patches of bacterial membrane lack lipid reservoirs at the edges, which may allow independent area expansion of each of the leaflets, thus uncoupling them. However, because the inner *E. coli* membrane is densely packed with integral proteins (50% by weight), it may be assumed that this greatly impedes slippage of the two leaflets, making this system similar to a closed liposome in terms of its response to amphipath incorporation.

Early data on the modulation of MscS-like channels by chlorpromazine, trinitrophenol, and lysophosphatidylcholine (LPC) showed that these substances invariably activate the

channels when presented from the cytoplasmic side (48). In this respect, the action of these amphipaths is distinct from the observed inhibitory action of TFE, which lowers the activation threshold only when presented to the periplasmic side. This difference is the focus of further investigation. A strong activating effect of externally applied lysolipids has also been reported for the large mechanosensitive channel MscL. Spontaneous activation was observed in the presence of large concentrations of LPC, an effect that only occurred when LPC is applied asymmetrically (49). In this regard LPC, like TFE, may strongly perturb leaflet area. However, it is not known if TFE causes the same spontaneous positive curvature, a feature characteristic of LPC.

The increased propensity to inactivation in the presence of TFE can be explained by partial separation of TM1-TM2 pairs from the gate-forming TM3 helices and stabilization of this state by intercalating TFE. As illustrated by data in Fig. 5, TFE does not drive MscS inactivation at low tension, thus its partitioning into the interhelical crevices (at low concentrations) does not seem to occur spontaneously. Instead, TFE partitioning appears to be critically facilitated by membrane tension that, in the framework of our gating hypothesis (Fig. 8), normally drives TM2-TM3 separation. TFE occupying voids in the molecule would stabilize the inactivated state, preventing fast reassociation of the TM1-TM2 pairs with TM3 and thus recovery (Fig. 6). Such an effect would also result in a less compact conformation of the MscS channel consistent with a slight upshift of MscS bands observed in gel electrophoresis upon addition of TFE (Fig. 1 C). The sidedness of the inactivating effect of TFE, shown to be active only from the cytoplasmic side (Figs. 2–44), supports the proposed location of the crevices as being accessible only from the cytoplasmic face. TFE added to the pipette does not cause inactivation, presumably because, after traversing the membrane core, it does not substantially accumulate in the cytoplasmic leaflet, as it would quickly partition out into the TFE-free aqueous compartment.

At the present stage we cannot firmly exclude that TFE in some way modifies the cytoplasmic “cage” domain leading to inactivation. It has been previously shown that the channel propensity to inactivation depends on the state of this cage domain, which can be altered either by truncating mutations (50) or by high-molecular-weight co-solvents (51). Additionally, it has been demonstrated that concentrations of TFE as low as 3–5 vol % can influence conformational distributions in soluble proteins (52,53). Besides the TM2-TM3 crevices, other apolar solvent-accessible areas of MscS, such as the pore vestibules (Fig. 7), could potentially act as sites of TFE accumulation. Although possible at higher concentrations, accumulation in the pore does not seem to occur in the tested range of 0.5–5 vol % as TFE was not observed to interfere with the single-channel conductance (Fig. 4, A and B, *inset*). The slow onset of TFE action on wash-in (Figs. 2 and 3) and slow return of channel activity on washout (Fig. 4 C) are also more consistent with TFE partitioning into and

out of a relatively large hydrophobic reservoir, a role more likely to be served by the membrane itself. A detailed comparison of the water-membrane partitioning coefficients with the concentration dependencies of their membrano-tropic actions for TFE and similar compounds is a current research focus and may clarify the above issues.

## CONCLUSIONS AND PROSPECTS

We have identified two ranges of concentrations for TFE, which cause separable effects on the MscS channel. The lower range (0.5–5 vol %) dramatically affects the kinetics of inactivation under tension with no effect on the oligomeric state of the channel complex. The higher range (10–15 vol %) causes larger perturbations, ultimately leading to subunit separation. The data above suggests that TFE can be used not only as a protein-denaturing proteomics tool, but also as a perturbing agent that biases membrane proteins toward specific conformational states or reduces transition barriers. We observed that the effects of TFE are consistent with the existing models of MscS activation and inactivation (26).

Future projects will certainly require a more quantitative analysis of TFE partitioning into cell membranes, liposomes, monolayers, and micelles and its effects on lateral pressure. A detailed kinetic analysis of MscS inactivation/recovery in the presence of different concentrations of TFE may suggest the characteristic times, distances, and pathways of TFE redistribution between the lipid bilayer and protein. Further understanding of the structural organization of MscS could be obtained by using TFE to probe the strength of inter-subunit interactions in mutants with perturbed or stabilized helical contacts, thus the location of crevices filled with TFE in the inactivated state can be further specified. Also, perturbing the tight TM3-TM3 knob-into-hole packing in the resting state (27,28) with mutations may weaken the complex against TFE. If a decrease in stability is not observed in such mutants, we should search for alternative intersubunit contacts, not seen in the delipidated crystal structure.

As more atomic structures of membrane proteins become available and more realistic force fields for molecular simulations are developed, the utilization of nonaqueous co-solvents will become more useful and interpretable. Parameters for MD simulations of proteins in the presence of TFE are already available (36,54). The merging of computation with experimental research will be a powerful strategy in studies of function-defining conformational transitions in membrane proteins.

## REFERENCES

1. Hong, D. P., M. Hoshino, R. Kuboi, and Y. Goto. 1999. Clustering of fluorine-substituted alcohols as a factor responsible for their marked effects on proteins and peptides. *J. Am. Chem. Soc.* 121:8427–8433.

2. Nelson, J. W., and N. R. Kallenbach. 1986. Stabilization of the ribonuclease S-peptide  $\alpha$ -helix by trifluoroethanol. *Proteins*. 1:211–217.
3. Sonnichsen, F. D., J. E. Van Eyk, R. S. Hodges, and B. D. Sykes. 1992. Effect of trifluoroethanol on protein secondary structure: an NMR and CD study using a synthetic actin peptide. *Biochemistry*. 31:8790–8798.
4. Wienk, H. L., M. Czisch, and B. de Kruijff. 1999. The structural flexibility of the preferredoxin transit peptide. *FEBS Lett.* 453:318–326.
5. Jasanoff, A., and A. R. Fersht. 1994. Quantitative determination of helical propensities from trifluoroethanol titration curves. *Biochemistry*. 33:2129–2135.
6. Luo, P., and R. L. Baldwin. 1999. Interaction between water and polar groups of the helix backbone: an important determinant of helix propensities. *Proc. Natl. Acad. Sci. USA*. 96:4930–4935.
7. Lu, H., M. Buck, S. E. Radford, and C. M. Dobson. 1997. Acceleration of the folding of hen lysozyme by trifluoroethanol. *J. Mol. Biol.* 265:112–117.
8. Kumar, Y., S. Muzammil, and S. Tayyab. 2005. Influence of fluoro, chloro and alkyl alcohols on the folding pathway of human serum albumin. *J. Biochem. (Tokyo)*. 138:335–341.
9. Chitra, R., and P. E. Smith. 2001. Properties of 2,2,2-trifluoroethanol and water mixtures. *J. Chem. Phys.* 114:426–435.
10. Cammers-Goodwin, A., T. J. Allen, S. L. Oslick, K. F. McClure, J. H. Lee, and D. S. Kemp. 1996. Mechanism of stabilization of helical conformations of polypeptides by water containing trifluoroethanol. *J. Am. Chem. Soc.* 118:3082–3090.
11. Kentsis, A., and T. R. Sosnick. 1998. Trifluoroethanol promotes helix formation by destabilizing backbone exposure: desolvation rather than native hydrogen bonding defines the kinetic pathway of dimeric coiled coil folding. *Biochemistry*. 37:14613–14622.
12. Bodkin, M. J., and J. M. Goodfellow. 1996. Hydrophobic solvation in aqueous trifluoroethanol solution. *Biopolymers*. 39:43–50.
13. Rajan, R., and P. Balaram. 1996. A model for the interaction of trifluoroethanol with peptides and proteins. *Int. J. Pept. Protein Res.* 48:328–336.
14. Reiersen, H., and A. R. Rees. 2000. Trifluoroethanol may form a solvent matrix for assisted hydrophobic interactions between peptide side chains. *Protein Eng.* 13:739–743.
15. Banerjee, T., and N. Kishore. 2005. Does the anesthetic 2,2,2-trifluoroethanol interact with bovine serum albumin by direct binding or by solvent-mediated effects? A calorimetric and spectroscopic investigation. *Biopolymers*. 78:78–86.
16. Cortes, D. M., and E. Perozo. 1997. Structural dynamics of the *Streptomyces lividans* K<sup>+</sup> channel (SKC1): oligomeric stoichiometry and stability. *Biochemistry*. 36:10343–10352.
17. van den Brink-van der Laan, V., J. Chupin, A. Killian, and B. de Kruijff. 2004. Stability of KcsA tetramer depends on membrane lateral pressure. *Biochemistry*. 43:4240–4250.
18. Barrera, F. N., M. L. Renart, M. L. Molina, J. A. Poveda, J. A. Encinar, A. M. Fernandez, J. L. Neira, and J. M. Gonzalez-Ros. 2005. Unfolding and refolding in vitro of a tetrameric,  $\alpha$ -helical membrane protein: the prokaryotic potassium channel KcsA. *Biochemistry*. 44:14344–14352.
19. Deshusses, J. M., J. A. Burgess, A. Scherl, Y. Wenger, N. Walter, V. Converset, S. Paesano, G. L. Cortals, D. F. Hochstrasser, and J. C. Sanchez. 2003. Exploitation of specific properties of trifluoroethanol for extraction and separation of membrane proteins. *Proteomics*. 3:1418–1424.
20. Zuobi-Hasona, K., P. J. Crowley, A. Hasona, A. S. Bleiweis, and L. J. Brady. 2005. Solubilization of cellular membrane proteins from *Streptococcus mutans* for two-dimensional gel electrophoresis. *Electrophoresis*. 26:1200–1205.
21. Spelbrink, R. E., A. Kolkman, M. Slijper, J. A. Killian, and B. de Kruijff. 2005. Detection and identification of stable oligomeric protein complexes in *Escherichia coli* inner membranes: a proteomics approach. *J. Biol. Chem.* 280:28742–28748.
22. Levina, N., S. Totemeyer, N. R. Stokes, P. Louis, M. A. Jones, and I. R. Booth. 1999. Protection of *Escherichia coli* cells against extreme turgor by activation of MscS and MscL mechanosensitive channels: identification of genes required for MscS activity. *EMBO J.* 18:1730–1737.
23. Sukharev, S. 2002. Purification of the small mechanosensitive channel of *Escherichia coli* (MscS): the subunit structure, conduction, and gating characteristics in liposomes. *Biophys. J.* 83:290–298.
24. Okada, K., P. C. Moe, and P. Blount. 2002. Functional design of bacterial mechanosensitive channels. Comparisons and contrasts illuminated by random mutagenesis. *J. Biol. Chem.* 277:27682–27688.
25. Koprowski, P., and A. Kubalski. 1998. Voltage-independent adaptation of mechanosensitive channels in *Escherichia coli* protoplasts. *J. Membr. Biol.* 164:253–262.
26. Akitake, B., A. Anishkin, and S. Sukharev. 2005. The “dashpot” mechanism of stretch-dependent gating in MscS. *J. Gen. Physiol.* 125:143–154.
27. Bass, R. B., P. Strop, M. Barclay, and D. C. Rees. 2002. Crystal structure of *Escherichia coli* MscS, a voltage-modulated and mechanosensitive channel. *Science*. 298:1582–1587.
28. Edwards, M. D., Y. Li, S. Kim, S. Miller, W. Bartlett, S. Black, S. Dennison, I. Iscla, P. Blount, J. U. Bowie, and I. R. Booth. 2005. Pivotal role of the glycine-rich TM3 helix in gating the MscS mechanosensitive channel. *Nat. Struct. Mol. Biol.* 12:113–119.
29. Anishkin, A., and S. Sukharev. 2004. Water dynamics and dewetting transitions in the small mechanosensitive channel MscS. *Biophys. J.* 86:2883–2895.
30. Sotomayor, M., and K. Schulten. 2004. Molecular dynamics study of gating in the mechanosensitive channel of small conductance MscS. *Biophys. J.* 87:3050–3065.
31. Fraczkiewicz, R., and W. Braun. 1998. Exact and efficient analytical calculation of the accessible surface areas and their gradients for macromolecules. *J. Comput. Chem.* 19:319–333.
32. Eisenberg, D., E. Schwarz, M. Komaromy, and R. Wall. 1984. Analysis of membrane and surface protein sequences with the hydrophobic moment plot. *J. Mol. Biol.* 179:125–142.
33. Humphrey, W., A. Dalke, and K. Schulten. 1996. VMD: visual molecular dynamics. *J. Mol. Graph.* 14:33–38.
34. Kanjilal, S., N. Taulier, J. Y. Le Huerou, M. Gindre, W. Urbach, and M. Waks. 2003. Ultrasonic studies of alcohol-induced transconformation in  $\beta$ -lactoglobulin: the intermediate state. *Biophys. J.* 85:3928–3934.
35. Stenberg, F., P. Chovanec, S. L. Maslen, C. V. Robinson, L. L. Ilag, G. von Hippel, and D. O. Daley. 2005. Protein complexes of the *Escherichia coli* cell envelope. *J. Biol. Chem.* 280:34409–34419.
36. Roccatano, D., G. Colombo, M. Fioroni, and A. E. Mark. 2002. Mechanism by which 2,2,2-trifluoroethanol/water mixtures stabilize secondary-structure formation in peptides: a molecular dynamics study. *Proc. Natl. Acad. Sci. USA*. 99:12179–12184.
37. White, S. H., and W. C. Wimley. 1999. Membrane protein folding and stability: physical principles. *Annu. Rev. Biophys. Biomol. Struct.* 28:319–365.
38. Popot, J. L., and D. M. Engelman. 2000. Helical membrane protein folding, stability, and evolution. *Annu. Rev. Biochem.* 69:881–922.
39. Ozdirekcan, S., D. T. Rijkers, R. M. Liskamp, and J. A. Killian. 2005. Influence of flanking residues on tilt and rotation angles of transmembrane peptides in lipid bilayers. A solid-state 2H NMR study. *Biochemistry*. 44:1004–1012.
40. Strandberg, E., S. Ozdirekcan, D. T. Rijkers, P. C. van der Wel, R. E. Koeppe, R. M. Liskamp, and J. A. Killian. 2004. Tilt angles of transmembrane model peptides in oriented and nonoriented lipid bilayers as determined by 2H solid-state NMR. *Biophys. J.* 86:3709–3721.
41. Spronk, S. A., D. E. Elmore, and D. A. Dougherty. 2006. Voltage-dependent hydration and conduction properties of the hydrophobic pore of the mechanosensitive channel of small conductance. *Biophys. J.* 90:3555–3569.

42. Miller, S., M. D. Edwards, C. Ozdemir, and I. R. Booth. 2003. The closed structure of the MscS mechanosensitive channel. Cross-linking of single cysteine mutants. *J. Biol. Chem.* 278:32246–32250.
43. Edwards, M. D., I. R. Booth, and S. Miller. 2004. Gating the bacterial mechanosensitive channels: MscS a new paradigm? *Curr. Opin. Microbiol.* 7:163–167.
44. Barry, J. A., and K. Gawrisch. 1994. Direct NMR evidence for ethanol binding to the lipid-water interface of phospholipid bilayers. *Biochemistry.* 33:8082–8088.
45. Koenig, B. W., and K. Gawrisch. 2005. Lipid-ethanol interaction studied by NMR on bicelles. *J. Phys. Chem. B.* 109:7540–7547.
46. Sheetz, M. P., and S. J. Singer. 1974. Biological membranes as bilayer couples. A molecular mechanism of drug-erythrocyte interactions. *Proc. Natl. Acad. Sci. USA.* 71:4457–4461.
47. Heerklotz, H. 2001. Membrane stress and permeabilization induced by asymmetric incorporation of compounds. *Biophys. J.* 81:184–195.
48. Martinac, B., J. Adler, and C. Kung. 1990. Mechanosensitive ion channels of *E. coli* activated by amphipaths. *Nature.* 348:261–263.
49. Perozo, E., A. Kloda, D. M. Cortes, and B. Martinac. 2002. Physical principles underlying the transduction of bilayer deformation forces during mechanosensitive channel gating. *Nat. Struct. Biol.* 9:696–703.
50. Schumann, U., M. D. Edwards, C. Li, and I. R. Booth. 2004. The conserved carboxy-terminus of the MscS mechanosensitive channel is not essential but increases stability and activity. *FEBS Lett.* 572:233–237.
51. Grajkowski, W., A. Kubalski, and P. Koprowski. 2005. Surface changes of the mechanosensitive channel MscS upon its activation, inactivation, and closing. *Biophys. J.* 88:3050–3059.
52. Qin, Z., and T. C. Squier. 2001. Calcium-dependent stabilization of the central sequence between Met<sup>76</sup> and Ser<sup>81</sup> in vertebrate calmodulin. *Biophys. J.* 81:2908–2918.
53. Main, E. R., and S. E. Jackson. 1999. Does trifluoroethanol affect folding pathways and can it be used as a probe of structure in transition states? *Nat. Struct. Biol.* 6:831–835.
54. Chitra, R., and P. E. Smith. 2001. A comparison of the properties of 2,2,2-trifluoroethanol and 2,2,2-trifluoroethanol/water mixtures using different force fields. *J. Chem. Phys.* 115:5521–5530.